# Effects of packing shape and density on magnetic behavior of MnBi powder

Puttamawan Juntree[1], Tanachat Eknapakul[2], Supree Pinitsoontorn[3] and Prayoon Songsiriritthigul[1,2*]

## Abstract

In this work, the M-H hysteresis curves of manganese bismuth (MnBi) were studied as a function of packing shape and density measured by Vibrating Sample Magnetometer (VSM). MnBi powders were successfully prepared by sintering under vacuum at sintering temperature of 325 $^{\circ}$C for 120 hrs at base pressure of $4\times10^{-8}$ mbar. The MnBi phase identification and concentration were characterized by X-ray diffraction. The MnBi powder particles with size of less than 20 μm, which used in this work, were obtained by ball milling and followed by grid sieving. MnBi samples with different packing shapes were prepared by varying sample lengths with a fixed packing density of 6.366 g/cm$^3$. In order to obtain the credible magnetic properties, the demagnetizing factor (N) was used to correct the hysteresis curves. The N value was estimated to be 0.416, 0.390, and 0.340 with corresponding energy product ($(BH)_{max}$) of 1.04, 1.10 and 0.92 MGOe at sample heights of 0.35, 0.25 and 0.15 cm, respectively. Samples with different packing densities were determined by filling the equivalent mass in different volumes. The corrected $(BH)_{max}$ values of 1.29, 1.54 and 1.12 MGOe were obtained in the samples with packing densities of 7.427, 5.305 and 3.183 g/cm$^3$, respectively. The M-H curves of MnBi with varied packing shapes were slightly different, while variations of MnBi with varied packing densities were obvious. The changes in hysteresis loop upon varying packing density could be explained by the bistable behavior. Their coercivity enhancements was ascribed by degree of particle rotation. Interestingly and unexpectedly, the maximum $(BH)_{max}$ was obtained at the measured length of 0.25 cm which may suggest the measurement optimization.

**Keywords**: MnBi, energy product, VSM, demagnetizing factor

[1] Suranaree University of Technology and Synchrotron Light Research Institute

[2] Thailand Center of Excellence in Physics, MHESRI

[3] Institute of Nanomaterials Research and Innovation for Energy, Khon Kaen University

[*] Corresponding author. E-mail: py.song@sut.ac.th

Received: March 14, 2022; Revised: May 18, 2022; Accepted: July 4, 2022

## Introduction

Permanent magnets play an important role in modern technologies related to energy conversion (Songsiriritthigul, 2020). High performance permanent magnets are made of rare earth materials including Nd-Fe-B and Sm-Co magnetic materials. The aforementioned substance had a high maximum energy product $(BH)_{max}$, almost 60 MGOe (Mohapatra, & Liu, 2018). Materials containing these rare-earth elements, on the other hand, have apparent drawbacks, such as poor corrosion resistance and magnetic property loss as the temperature increases (Li et al., 2018). In addition, rare-earth elements, especially Nd and Sm, which are presented in the supply crisis and mining mobilization, will lead to environmental problems. To avoid such problems, rare-earth free permanent magnets are therefore an option even though the $(BH)_{max}$ of the theoretical predictions for rare-earth free magnetic materials, which are smaller than that of rare-earth magnetic materials. However, the above-mentioned drawbacks give extra motivation for rare-earth free permanent magnet research and development (Patel, Zhang, & Ren, 2018). Early production of permanent magnets was made of rare earth materials, such as Alnico and Ferrite magnets. The maximum energy product $(BH)_{max}$ value of such magnets is relatively low (Rani, Taya, & Kashyap, 2018). Because of its low material cost, manganese bismuth (MnBi) is an attractive rare-earth-free permanent magnetic material and its unusual magnetic properties, such as good magnetization at room temperature (Jensen et al., 2019) and high magneto-crystalline anisotropy. Low- temperature phase MnBi (LTP-MnBi) magnetic materials are interesting both in theory and in practice because of its large positive temperature coefficient of coercivity and high Curie temperature (Songsiriritthigul, 2020).

The fact that extremely large discrepancy of $(BH)_{max}$ of MnBi samples was reported (1.53-8.4 MGOe (Poudyal et al., 2016; Cao et al., 2019)) even the samples were prepared with rather the same approaches. According to our recent published work (Borsup et al., 2022), the $(BH)_{max}$ of up to 2.84 MGOe was observed in 59.50% MnBi content, which is relatively low compared to other works (Cao et al., 2019). In addition to the low MnBi content, the VSM measurement optimization and proper data correction shall be taken into account to reveal the precise magnetic performance of our MnBi.

In fact, the VSM is an open-loop measurement resulting in the distorted magnetic values (Dodrill, & Kelley, 2003). The simple magnetizing field correction which considers only the shape of the sample may be sufficient

to correct the data taken from VSM (Prozorov, & Kogan, 2018). By implementing the demagnetizing field correction, the open-loop can transform into close-loop, which is geometrical independent.

Motivated by the doubt that the experimental setup could affect the magnetic behavior, the effects of packing shape and density on magnetic behavior of MnBi have been studied. We showed here that the magnetic behavior significant changes by varying shape and density. Moreover, the reported $(BH)_{max}$ of our previous MnBi could be improved by 12% in the optimized conditions.

## Methodology

### 1. Preparation of LTP-MnBi

The raw materials in this research were high-purity Mn powders (99+%, size<420 microns)) and Bi powders (99.50%, size < 149 microns) purchased from Acros Organics. Mn powder was ball-milled for 3 hours in a planetary micro mill, then sieved to select Mn powder with a particle size of less than 20 μm. The Mn and Bi powders were mixed with a 1:3 atomic ratio and then sintered in a quartz tube of the effusion cell (Dr. Eberl MBE-Komponenten GmbH, NTEZ40-10-22-KS-HL-2118521). The base pressure of this system was maintained better than $4\times10^{-8}$ mbar. After that, the sintering temperature was set to 325°C with temperature increment of 5°C/min. The sintering process was taken place for 120 hours and then cooled down naturally to room temperature. The sintered samples were crushed and grinded to powder followed by ball milling. The particle sizes of less than 20 μm were chosen for further study. X-ray diffraction with Cu Kα radiation (λ=1.5406 Å) was used for phase identification operating at 30 kV and 10 mA. The 2θ was ranged from 20° to 60°. The magnetic properties had been investigated by using Vibrating Sample Magnetometer (VSM, Quantum Design, VersaLab located at Khon Kaen University) with applied magnetic field between -30 and +30 kOe. We noted here that there were some unreacted Mn particles which may result from the incomplete diffusion process in the stoichiometric condition (Borsup et al., 2022). Hence, more Bi was added to compensate for the MnBi formation during sintering. Actually, the research was planned to perform further processes such as magnetic separation. Indeed, the low MnBi concentration and low magnetic properties observed in this 1:3 atomic ratio was expected in the non-stoichiometric condition. We would like to emphasize that this ferromagnetic substance was valid to be performed in this study, which was independent of the initial magnetic properties.

## 2. Sample preparation for VSM measurements

In order to measure the magnetic properties of the powder samples, the standard cylindrical Quantum Design VSM holders (P125E) with 2 mm in diameter (2a) and 6 mm in length (2b) were used, showing the crucial parameters for magnetic correction. The demagnetizing factor (N) was determined from a cylinder in transverse magnetic field with equation (1)

$$N^{-1} = 2 + \frac{1}{\sqrt{2}}\frac{a}{b} \quad (1)$$

Where $a$ is the diameter and $b$ is the length (Coey, 2010; Prozorov, & Kogan, 2018; Qian et al., 2020). It should be noted that all data shown in this manuscript were corrected by the demagnetizing factor (N) and subtracted by the paramagnetic-like background to get the saturated Ms. In this work, the measurements had been divided into two parts. The measurements had been repeated for three times on the same set of the sample to avoid the effect of inhomogeneity, giving the error bar of up to 4%.

### 2.1 Samples with different packing shapes

Samples with three different shapes and fixed mass density were prepared by filling MnBi powder in the standard VSM sample holder with different amounts to yield packing density of 6.366 g/cm$^3$ (0.2 g/cm). This led to three different lengths or shapes and, thus, different N values. The MnBi amounts were 0.07 g, 0.05 g and 0.03 g, resulting in samples with three different lengths as shown in (Figure 1a-c). The N values could be calculated to be 0.416, 0.390 and 0.340 for the MnBi mass of 0.07 g (MnBi_S_1), 0.05 g (MnBi_S_2) and 0.03 g (MnBi_S_3), respectively.

### 2.2 Samples with different packing densities

Three samples with different masses were filled in the VSM sample holder with the same length giving different packing densities (Figure 1d-f). By this way, the N value was the same, which was calculated through the geometric shape to be 0.405. In details, 0.07 g (MnBi_D_1), 0.05 g (MnBi_D_2) and 0.03 g (MnBi_D_3) of MnBi powder were filled and gently pressed in a cylindrical holder with length of 0.30 cm leading to packing densities of 7.427, 5.305 and 3.183 g/cm$^3$, respectively. It was noted that the packing density was different from the material density (ρ).

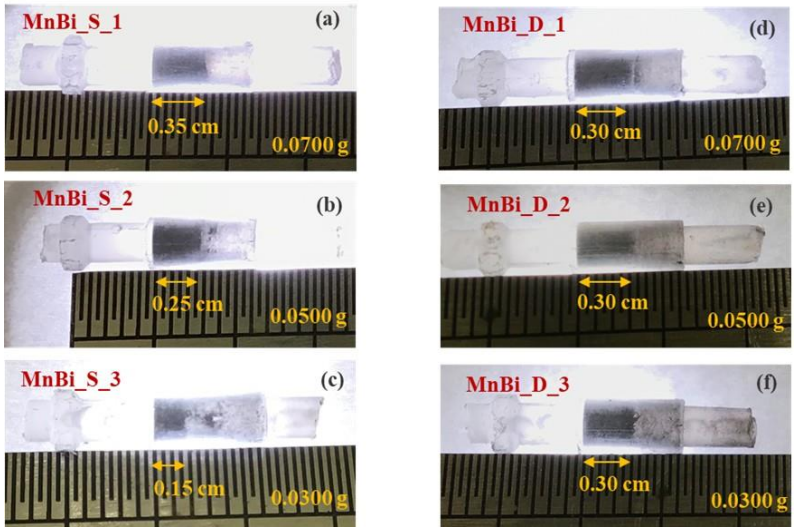


**Figure 1** (a, b and c) Samples with varied packing shape, and (d, e and f) samples with varied packing density.

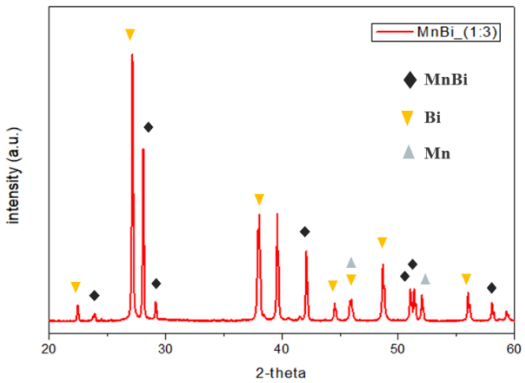


**Figure 2** The XRD patterns of MnBi with 3:1 (Bi:Mn) atomic ratio sintering at 325°C for 120 hrs. The MnBi particle size was less than 20 μm.

## Results and discussion

### 1. Phase identification of MnBi

(Figure 2) shows the XRD pattern of the sintered MnBi, indicating three main compositions, i.e., LTP-MnBi (card No. 96–900-8900), Mn (card No. 96–101-0394), and Bi (card No. 96–231-0890) with tiny oxide peaks (not identified). While there were only MnBi and Bi that appeared as main peaks, the MnBi and Bi ratios were then calculated from the intensity of the highest peaks (28.08° and 27.14°) to be 42.09% and 57.91%, respectively. It could be seen that there were relatively high Bi content as measured from the XRD pattern. This could be understood by the original 3:1 (Bi:Mn) atomic ratio used during the preparation process. which was found to have a large amount of Bi suggesting that Bi filtration was

needed to obtain higher MnBi purity. As a result, an excess of paramagnetic Bi made the suppression of overall magnetic performance. The Mn peaks were relatively low. This might be understood that the remaining un-reacted Mn exists as a core surrounded by the MnBi layer and, thus, all Mn could not be probed due to the limit of X-ray penetration depth (Nguyen, Jin, & Berkowitz, 2013).

**2. Effects of packing shape on magnetic properties**

As described in the experimental section, the MnBi samples were compressed with different lengths resulting in different N values for a constant packing density (Coey, 2010; Prozorov, & Kogan, 2018; Qian et al., 2020). It should be noted that samples used throughout experiment were the same, hence, the magnetic properties after magnetic field correction should be equaled. This intuitively means that an increase of N will give worse magnetic performance of the raw VSM data.

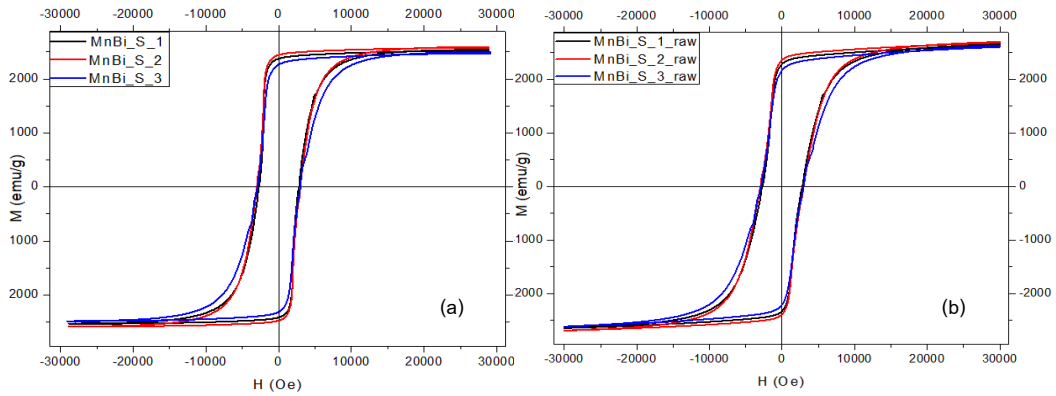


**Figure 3** (a) The corrected M-H hysteresis curves of the samples prepared in different packing shape. (b) The demagnetizing field uncorrected M-H curves of the MnBi with different packing shapes.

The demagnetizing field corrected M-H curves of the MnBi with different packing shapes (Figure 3a). The measured coercivity ($H_c$) of all samples were more or less identical with a value of circa 2.78-3.01 kOe. It was obvious that the MnBi_S_2 (red curve) exhibits the highest saturation magnetization ($M_s$) of about 2.59 emu/g. The MnBi_S_1 and MnBi_S_2 showed slightly smaller $M_s$ of 2.53-2.49 emu/g, respectively. The $(BH)_{max}$ was calculated to be 1.31, 1.39 and 1.14 MGOe for MnBi_S_1, MnBi_S_2 and MnBi_S_3, respectively. It was apparently seen that the experimental data were not consistent with the expectation. The corrected $(BH)_{max}$ of the MnBi_S_2 was 5.80% and 12% greater than MnBi_S_1 than MnBi_S_3, respectively. The

demagnetizing field uncorrected M-H curves of the MnBi with different packing shapes were shown in (Figure 3b). The $(BH)_{max}$ was calculated to be 1.04, 1.10 and 0.92 MGOe for MnBi_S_1_raw, MnBi_S_2_raw and MnBi_S_3_raw, respectively. It was found that the $(BH)_{max}$ after demagnetizing field correction data were better than the uncorrected ones (Prozorov, & Kogan, 2018). This means that the magnetic performance reported in (Borsup et al., 2022) might be enhanced by 12% when measured in the optimize conditions. Packing shapes with different lengths will result in different loops because the bistable behavior is partially inhibited in shorter packing shapes with larger demagnetization fields, which stops the magnetization jump on the way and gives rise to a qualitatively different loop (Bertotti, 1998). We expected that the $(BH)_{max}$ after correction should be the same. This means the raw $(BH)_{max}$ of the taller sample should be lower according to the theoretical higher N. However, the experimental results did not exhibit that kind of trend, which could be due to the setup optimization or the substance's inhomogeneity.

### 3. Effects of packing density on magnetic properties

In this section, the packing shape was fixed leading to constant N in all samples (Coey, 2010; Prozorov, & Kogan, 2018; Qian et al., 2020). While the mass used was varied resulting in different packing densities. As shown in (Figure 4), distinct M-H curves were obtained from samples with different packing densities. The $H_c$ of 2.79, 1.43 and 0.47 kOe were recorded for MnBi_D_1, MnBi_D_2, and MnBi_D_3, respectively. The $M_s$ was insignificant different for all samples, which were measured to be in arrange of 2.36 - 2.74 emu/g. The $(BH)_{max}$ values were calculated to be 1.29, 1.54 and 1.12 MGOe for MnBi_D_1, MnBi_D_2 and MnBi_D_3, respectively.

The higher $H_c$ found in higher packing density could be described by the degree of particle rotation (Vickers, 2017; Li et al., 2018). It was found that, in the varied packing density condition, the MnBi_D_2 exhibited the highest $(BH)_{max}$ value. This is surprisingly similar to the case of MnBi_S_2 obtained in varied packing shape conditions. This might be implied that the 0.05 g of MnBi was an optimizing value for this VSM system. The corrected magnetic properties of all samples are summarized in (Table 1).

**Table 1** Magnetic properties after demagnetizing field correction of all samples.

| sample ID | $H_c$ (kOe) | $M_s$ (emu/g) | $BH_{max}$ (MGOe) |
|---|---|---|---|
| MnBi_S_1 | 2.78 | 2.53 | 1.31 |
| MnBi_S_2 | 3.01 | 2.59 | 1.39 |
| MnBi_S_3 | 2.95 | 2.49 | 1.14 |
| MnBi_D_1 | 2.79 | 2.50 | 1.29 |
| MnBi_D_2 | 1.43 | 2.74 | 1.54 |
| MnBi_D_3 | 0.47 | 2.36 | 1.12 |

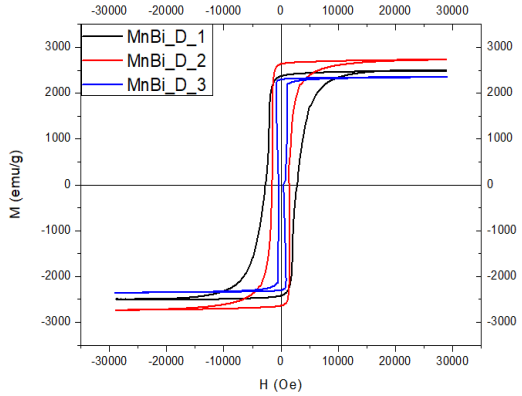


**Figure 4** The corrected M-H hysteresis curves of the samples prepared in different packing densities.

## Conclusion

This work demonstrates the impact of the VSM sample preparation to the measured magnetic properties of MnBi powder. Firstly, slightly different magnetic properties were found in the samples with different packing shape. However, it was worth noting that the change in the magnetic properties did not follow the predicted trend of the demagnetizing field correction. The highest $(BH)_{max}$ value was obtained from the 0.05 g samples in both cases, which could be implied by the optimizing system condition or the sample's inhomogeneity. Secondly, the changes of MnBi with different packing densities, especially the $H_c$ value, were obvious, which could be described by the bistable behavior and a degree of particle rotation. The results of this work emphasize that careful measurements were required in order to obtain the maximize and credible magnetic properties taken from VSM.

## Acknowledgement

This work was supported by the Thailand Center of Excellence in Physics and the Research Network NANOTEC (RNN) program of the National Nanotechnology Center (NANOTEC) of Thailand.

## References

Bertotti, G. (1998). *Hysteresis in magnetism: for physicists, materials scientists, and engineers*. San Diego: Academic Press.

Borsup, J., Eknapakul, T., Myint, H. T., Smith, M. F., Yordsri, V., Pinitsoontorn, S., ... & Songsiriritthigul, P. (2022). Formation and magnetic properties of low-temperature phase manganese bismuth prepared by low-temperature liquid phase sintering in vacuum. *Journal of Magnetism and Magnetic Materials*, *544*, 168661.

Cao, J., Huang, Y. L., Hou, Y. H., Shi, Z. Q., Yan, X. T., Zhong, Z. C., & Wang, G. P. (2019). Microstructure and magnetic properties of MnBi alloys with high coercivity and significant anisotropy prepared by surfactant assisted ball milling. *Journal of Magnetism and Magnetic Materials*, *473*, 505-510.

Coey, J. M. (2010). *Magnetism and magnetic materials*. Cambridge: Cambridge university press.

Dodrill, B. C., & Kelley, B. J. (2003). *Measurements with a VSM: Permanent magnet materials*. Retrieved February 6, 2022, from http://www. lakeshore.com/ Documents/Permanent%20Magnet%20Paper. pdf.

Jensen, B. A., Tang, W., Liu, X., Nolte, A. I., Ouyang, G., Dennis, K. W., & Cui, J. (2019). Optimizing composition in MnBi permanent magnet alloys. *Acta Materialia*, *181*, 595-602.

Li, B., Ma, Y., Shao, B., Li, C., Chen, D., Sun, J., ... & Yin, X. (2018). Preparation and magnetic properties of anisotropic MnBi powders. *Physica B: Condensed Matter*, *530*, 322-326.

Mohapatra, J., & Liu, J. P. (2018). Rare-earth-free permanent magnets: the past and future. *Handbook of magnetic materials*, *27*, 1-57.

Nguyen, P. K., Jin, S., & Berkowitz, A. E. (2013). Unexpected magnetic domain behavior in LTP-MnBi. *IEEE transactions on magnetics*, *49*(7), 3387-3390.

Patel, K., Zhang, J., & Ren, S. (2018). Rare-earth-free high energy product manganese-based magnetic materials. *Nanoscale*, *10*(25), 11701-11718.

Poudyal, N., Liu, X., Wang, W., Nguyen, V. V., Ma, Y., Gandha, K., ... & Cui, J. (2016). Processing of MnBi bulk magnets with enhanced energy product. *AIP Advances, 6*(5), 056004.

Prozorov, R., & Kogan, V. G. (2018). Effective demagnetizing factors of diamagnetic samples of various shapes. *Physical Review Applied*, *10*(1), 014030.

Qian, H. D., Yang, Y., Lim, J. T., Kim, J. W., Choi, C. J., & Park, J. (2020). Effects of Mg and Sb substitution on the magnetic properties of magnetic field annealed MnBi alloys. *Nanomaterials*, *10*(11), 2265.

Rani, P., Taya, A., & Kashyap, M. K. (2018). Enhancement of magnetocrystalline anisotropy of MnBi with Co interstitial impurities. *AIP Conference Proceedings*, *1942*(1), 130033.

Songsiriritthigul, P. (2020). Advances in permanent magnets free of rare earth elements: manganese-bismuth. *Thai Journal of Physics*, *37*(2), 60-73.

Vickers, N. J. (2017). Animal communication: when i'm calling you, will you answer too?. *Current biology*, *27*(14), R713-R715.